Phys Chem Minerals (2006) 33: 426–434
DOI 10.1007/s00269-006-0087-9

ORIGINAL PAPER

Geoffrey David Bromiley · Andrei A. Shiryaev

Neutron irradiation and post-irradiation annealing of rutile (TiO_{2-x}): effect on hydrogen incorporation and optical absorption

Received: 19 July 2005 / Accepted: 26 April 2006 / Published online: 30 May 2006

Abstract Neutron irradiation and post-irradiation annealing under oxidising and reducing conditions have been used to investigate H incorporation in, and the optical properties of, reduced (TiO_{2-x}) rutile. Optical absorption in rutile is mainly due to a Ti^{3+} Ti^{4+} intervalence charge transfer effect. The main mechanism for H incorporation in rutile involves interstitial H not coupled to other defects, which has important implications for the rate of H diffusion, and possibly also on the electrical properties of rutile. Additional minor OH absorption bands in IR spectra indicate that a small amount of interstitial H is coupled to defects such as Ti^{3+} on the main octahedral site, and indicates that more than one H incorporation mechanism may operate. Concentration of oxygen vacancies has a controlling influence on the H affinity of rutile.

Keywords Hydrogen · Rutile · Spectroscopy · Neutron irradiation · Radiation defects

Introduction

The incorporation of trace amounts of hydrogen in nominally anhydrous mantle phases can affect a wide range of mineral and bulk mantle properties, from electrical conductivity to rheology, and may represent an important mechanism for incorporating significant volumes of water in the deep interior of the Earth. The most commonly used methods to determine H incorporation mechanisms include FTIR and NMR spectroscopy (e.g. Kohn et al. 2002; Katayama et al. 2003; Bromiley and Keppler 2004). The results of studies utilising these techniques demonstrate that H is usually incorporated in nominally anhydrous minerals (NAMs) at interstitial sites associated with specific oxygen anions. These techniques can be used to provide information on local environments surrounding interstitial H cations, and if sufficient additional information is available, data may be used to propose potential H sites in the host structure and how H incorporation is charge balanced. A more powerful technique to study H incorporation is neutron diffraction. This can be used to directly refine either hydrogen or deuterium positions (e.g. Swope et al. 1995; Lager and Von Dreele 1996). However, it has certain limitations that prevent widespread use, most notably that relatively large sample volumes are required. Also, the overall 'water' content of samples has to be relatively high, and measurements can only be made at large scale facilities. All these commonly used techniques share one major limitation. Whilst they provide direct or indirect information on H positions, they often do not provide much, or any information on how interstitial H interacts with other defects in the host phase.

Irradiation of materials with high energy particles is a well established tool in solid state chemistry, condensed matter physics and materials science, where it is used to investigate the nature of defects and defect clusters in a broad range of materials (e.g. Lehman 1977). In this technique, high-energy particles (e.g., neutrons, electrons, ions) are used to bombard a sample material and create a range of different defects. Vacancies and interstitials are the main primary radiation defects formed. These may be relatively short-lived, and may be destroyed by interaction with other defects. However, some of them persist in the sample material. The effects of such defects on mineral properties, and the interaction of different types of defects can then be studied. Additional annealing experiments can also be performed

G. D. Bromiley
Bayerisches Geoinstitut, Universität Bayreuth,
Bayreuth, Germany

G. D. Bromiley (✉)
Department of Earth Sciences, University of Cambridge,
Downing Street, Cambridge CB2 3EQ, UK
E-mail: gbro04@esc.cam.ac.uk
Tel.: +44-1223-333464
Fax: +44-1223-333450

A. A. Shiryaev
A.V. Shubnikov Institute of Crystallography RAS,
Leninsky Pr. 59, 119333 Moscow, Russia

on irradiated samples. Investigations of H incorporation in NAMs have demonstrated that H usually interacts with other types of defect such as substitutional defects (lower valence cation substitutions), cation or anion vacancies or with other interstitial H (e.g. the formation of clusters or pairs of OH groups). The effect of H incorporation on mineral properties is likely to be strongly constrained by the degree of interaction between interstitial H and other point defects in the host phase. In this paper, we explore the possibility of using neutron irradiation and post-irradiation annealing to provide additional information on how H interacts with other defects in a commonly studied NAM, rutile, and on the relative stability of different H-related defects and defect clusters.

Experimental details

Rutile was synthesised at 1.5 GPa, 1,500°C for 48 h under water-saturated conditions using 0.75″ end-loaded piston-cylinder apparatus. High-purity TiO_2 (rutile) (99.998% Chempure) was loaded into a Pt capsule with 5 wt% distilled H_2O, which was then welded shut. The capsule was placed in a pyrophyllite sleeve and loaded into a 0.75″ talc-pyrex sample assembly. After the run, the capsule was pierced to check for the presence of water. The sample was recovered as small, subhedral to euhedral, dark blue–black crystals of rutile, which were typically elongated along [001], and which ranged up to 80 μm in length and a few tens of microns in other directions. Optical, micro-Raman and powder-XRD examination of the sample demonstrated that all crystals were rutile and that no additional phase was present. The sample was divided into three separate batches.

Rutile samples were irradiated using a reactor at the Moscow Engineering Physics Institute. Neutrons from the reactor have a decay energy spectrum with average energy of ≈2 MeV. The fluence at the sample was 1.1×10^{13} neutrons/cm^2/s. It is important to note that energetic neutrons penetrate throughout the bulk of irradiated samples, creating a uniformly distributed damage. Samples were irradiated for 13–16 h. Three batches of the sample were prepared. One batch was irradiated once (total flux of around 10^{16} neutrons/cm^2), and a second batch was irradiated twice (total flux around 2×10^{16} neutrons/cm^2). A third batch of the samples was not irradiated, but was kept for comparison. During annealing, samples were wrapped in Al foil, and individual crystals were randomly orientated. Sample temperature during irradiation was kept below 60°C.

Irradiated and non-irradiated crystals were prepared for examination using FTIR and Raman spectroscopy. Due to the euhedral nature of some of the crystals, orientation could be established optically. Samples were mounted in Crystalbond™ and prepared as doubly polished plates approximately 30 μm thick. Raman spectra were taken using a benchtop Dilor Labram Raman spectrometer equipped with a 20 mW HeNe laser and a microscope. Sample plates were then removed from their glass slides for FTIR analysis by soaking in high-purity acetone for 24 h. Near-infrared spectra were taken using a Bruker IFS 120 HR high-resolution FTIR spectrometer coupled with a Bruker IR microscope containing all-reflecting Cassegranian optics and a permanently aligned Michelson-type interferometer with a 30° angle of incidence on the beam splitter. Measurements were taken using a tungsten light source, a Si-coated CaF_2 beamsplitter and a narrow-band MCT detector. Further details of the IR setup are given in Bromiley et al. (2004b). H contents (expressed as ppm H_2O by weight) of the samples were calculated using the Beer–Lambert law on species absorption and the IR integral absorption coefficients determined by Hammer and Beran (1991).

Neutron irradiation of reduced rutile

The effects of neutron irradiation on the optical properties of the rutile samples are quite pronounced. Before irradiation, rutile crystals were dark blue. After one dose of irradiation, crystals were light blue; after two doses, rutile crystals were pale yellow. Figure 1 shows NIR spectra obtained from unirradiated and irradiated rutile samples, and Fig. 2 shows an enlarged view of the NIR spectra showing the region of absorption due to the presence of structurally-incorporated hydrogen. Raman spectra obtained from rutile before and after irradiation are shown in Fig. 3.

Optical properties

Broad optical absorption in non-stoichiometric rutile is explained by two contrasting models (see Khomenko et al. (1998) and references therein): (1) Absorption due to a polaron effect resulting from the trapping of a pair

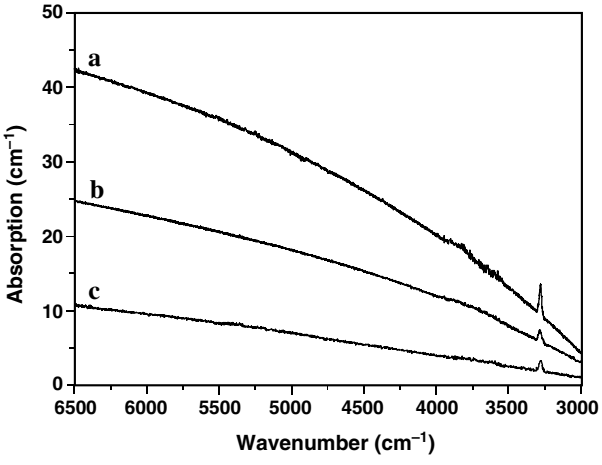

Fig. 1 Unpolarised NIR spectra from rutile (TiO_{2-x}) samples *a* before irradiation, *b* after irradiation and *c* after two doses of neutron irradiation. Spectra are offset vertically for clarity

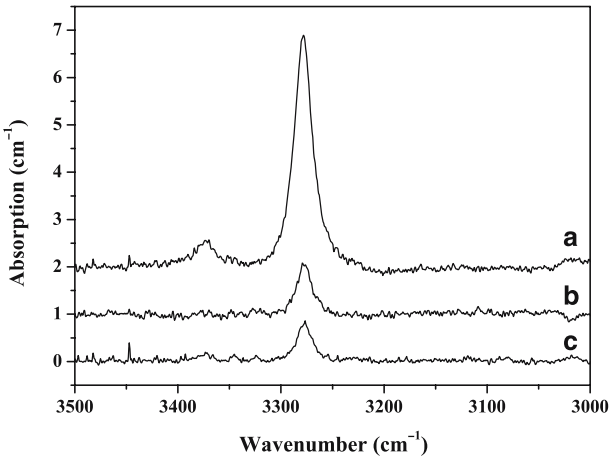

Fig. 2 Expanded section of the NIR rutile spectra showing OH stretching absorption bands. A flat background over the OH region has been subtracted. Labelling as in Fig. 1

of electrons at an oxygen vacancy, and (2) Absorption due to Ti^{3+} Ti^{4+} intervalence charge transfer (IVCT), where an electron is shared between Ti cations on adjacent interstitial and octahedral sites in the rutile structure, coupled with Ti^{3+} crystal field transitions. The difference between these models is important because they either imply that oxygen vacancies ($V_O^{\cdot\cdot}$) or interstitial Ti^{3+} ($Ti_i^{\cdot\cdot\cdot\cdot}$) are the dominant intrinsic defect species in non-stoichiometric or reduced rutile, using Kröger and Vink (1956) notation. Figure 4 shows a representation of the rutile structure showing some of the important defects likely to be stable in reduced, H-bearing rutile.

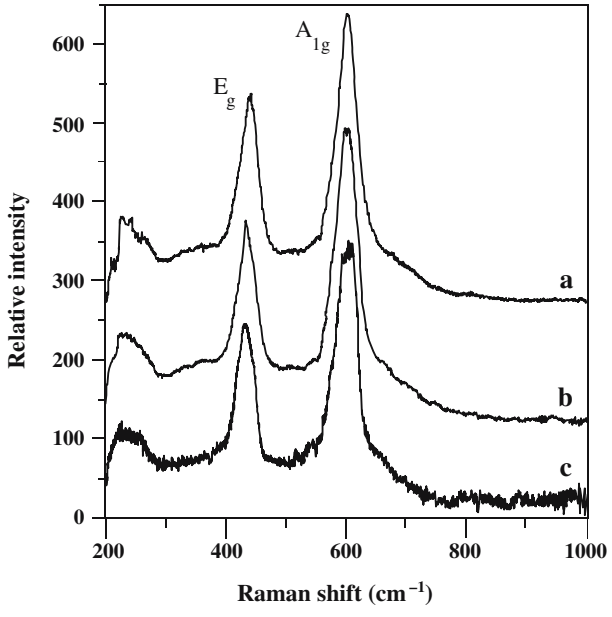

Fig. 3 Raman spectra from rutile *a* before irradiation, *b* after irradiation and *c* after two batches of irradiation. Labelling as in Fig. 1

The main effect of neutron irradiation of oxides is production of $V_O^{\cdot\cdot}$, due to the typically low displacement threshold energies of anions (e.g. Kappers 1978), which is mainly related to the relative size and charge of anions in crystal structures. In rutile, displacement energies for O in rutile are approximately two times smaller than for Ti (Buck 1995; Thomas et al. 2005), which should strongly favour formation of $V_O^{\cdot\cdot}$ over Ti vacancies. It is possible to use Raman spectroscopy to provide direct evidence for the formation of oxygen vacancies in rutile during neutron irradiation (Lu et al. 2002a). Raman spectra from TiO_2 rutile contain two prominent Raman modes: E_g (447 cm^{-1}) parallel to [001] and A_{1g} (612 cm^{-1}) perpendicular to [001], as well as a small broad peak around 232 cm^{-1} due to a mixed phonon process. Relative shifts in the wavenumber and intensities of these bands can be related to formation of oxygen vacancies. The E_g Raman mode is related to vibration of two oxygen ions per unit cell at the C_4 axis of an octahedron (Traylor et al. 1971). Loss of one of these oxygens will markedly affect the intensity and frequency of the E_g mode. However, the A_{1g} mode is related to movement of all six oxygens, so will be less strongly affected by oxygen loss from the structure relative to the E_g mode. Lu et al. (2002a) noted that production of oxygen vacancies during neutron irradiation of stoichiometric rutile (TiO_2) resulted in a shift in the E_g band to slightly lower wavenumbers and a marked reduction in intensity relative to the A_{1g} band. A similar trend is noted following irradiation of reduced rutile in this study (Fig. 4), although the trend is less clear due to a poorer signal to noise ratio resulting from smaller sample size, as well as the fact that the rutile samples were grown under reducing conditions to begin with.

The effect of neutron irradiation on reduced rutile is to lower the amount of optical absorption. It is possible to see this effect in NIR spectra (Fig. 1), because the broad optical absorption characteristic of reduced rutile extends far into the near-infrared part of the spectrum, and is seen as steep negatively sloping backgrounds on NIR spectra. As the main result of neutron irradiation is production of oxygen vacancies, we must conclude that optical absorption in reduced rutile is due to mechanism (2), that is, mainly due to Ti^{3+} Ti^{4+} IVCT. If optical absorption were due to electron trapping at oxygen vacancies (i.e. the formation of F and F+ centres), then irradiation would result in an increase in optical absorption. Instead, creation of oxygen vacancies is somehow related to a decrease in the amount of interstitial Ti^{3+}. Loss of interstitial Ti^{3+} could be due to an increase in the amount of O bonding (in terms of the sum of the Pauling bond strengths) and charge-imbalance resulting from loss of O. Interstitial Ti^{3+} could be removed by bulk transport of Ti defects to the rutile surface, as has been observed experimentally observed during oxidation experiments on non-stoichiometric rutile (Diebold 2003), or by recombination of interstitial Ti^{3+} with Ti vacancies (i.e. $V_{Ti}^{////}$), another defect which may be present in strongly reduced rutile, and which

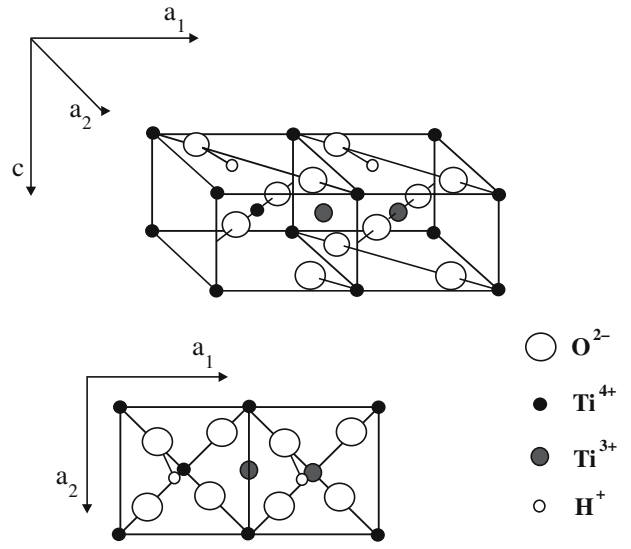

Fig. 4 Three-dimensional view (*above*) and corresponding 2D representation (*below*) of part of the rutile structure showing some of the important defects expected in reduced rutile. Figure shows interstitial H (incorporated via the Swope et al. (1995) model) uncoupled from other defects (*left*), and coupled to reduced Ti on an adjacent octahedral site (*right*), a Ti^{3+} interstitial and an oxygen vacancy (*left*). Adapted from Aono and Hasiguti (1993)

could also be formed during neutron irradiation. Additionally, a minor amount of interstitial Ti may also be directly lost during neutron bombardment.

After prolonged neutron irradiation, rutile crystals are yellow. After annealing in air at 1,000°C for 30 min, these crystals become colourless. Unfortunately, due to size limitations, we were unable to obtain good quality optical spectra from the rutile samples. The yellow colour could be due to trapping of electron pairs at oxygen vacancies or due to crystal field transitions in octahedrally coordinated Ti^{3+} (i.e. Ti'_{Ti}), with no additional absorption due to IVCT because of an absence of interstitial Ti.

H incorporation

NIR spectra from unirradiated rutile (Fig. 2) contain two OH stretching bands at 3,279 and 3,375 cm^{-1}. On the basis of neutron diffraction data, Swope et al. (1995) suggested that H docks close to (1/2 1/2 0) in the rutile structure, with vibration of the OH dipole just off of a shared octahedral edge (as shown in Fig. 4). Bromiley and Hilaret (2005) suggested that the IR band in rutile spectra at 3,279 cm^{-1} is due to H incorporated at this interstitial site ($H_i^{\cdot}$), either associated with a Ti^{3+} substitutional defect on an adjacent octahedral site (Ti'_{Ti}), or H uncoupled to any other defects. Lu et al. (2002b) and Khomenko et al. (1998) both noted the presence of an additional, small OH band at 3,326–3,327 cm^{-1} in rutile spectra, which they interpreted as evidence for OH–O bonding or H coupled with octahedral Ti^{3+} (Ti'_{Ti}), respectively. Differences between published spectra and those presented here probably relate to differences in sample preparation (P–T–fO_2 conditions of synthesis and reduction via proton implantation), and may in turn be related to redox conditions during synthesis or annealing.

Neutron irradiation reduces H affinity in rutile. After irradiation, the height of the main OH band at 3,279 cm^{-1} is markedly reduced, and the small additional band at 3,375 cm^{-1} is no longer present. After a second dose of irradiation, the height of the main OH band is, probably, reduced slightly further. Total water contents of rutile are 93 ± 19 ppm H_2O weight before irradiation, and 14 ± 3 and 11 ± 2 ppm H_2O weight, after one and two doses of irradiation, respectively. H loss can also be related to loss of oxygen during irradiation resulting in an increase in O overbonding and lowering of H affinity, and/or neutron irradiation resulting in the creation of $V_O^{\cdot\cdot}$, charge imbalance, and accommodation by loss of H. More directly, neutron irradiation could also lead to the direct breaking of O–H bonds if the O anion involved in the bond was removed during irradiation. H loss following breaking of O–H bonds has been observed during electron irradiation of rutile (Gonzalez and Chen 2002). However, the most important point to note is that neutron irradiation does not appear to fundamentally affect the mechanism for H incorporation in rutile that gives rise to the OH band at 3,279 cm^{-1}. No shift in frequency of this band to higher or lower wavenumbers after irradiation is noted.

Post-irradiation annealing

Experimental technique

For annealing experiments, we used an in-house built NIR-transparent microscope heating stage of the type described by Zapunnyy et al. (1989), which was mounted on the microscope stage of the infrared spectrometer described above. This heating stage contains a Pt resistance furnace (made from 0.1 mm thick Pt sheet), which was specially adapted to hold very small samples down to a few tens of microns in size. Samples were suspended over a small circular aperture in the furnace, with CaF_2 windows at the top and base of the unit allowing access to the IR beam. The heating stage also contains an outer cooling ring to prevent damage to the optics of the microscope and allow rapid quenching, as well as a small, hermetically sealed sample volume. Inlet and outlet valves to the sample volume allow the atmosphere to be carefully controlled by passing a stream of gas over the sample during heating. For the present study, we performed annealing experiments under oxidizing (air) and reducing (Ar–2%H_2 gas mixture) conditions. A Pt–10%Rh thermocouple (S type) was used to monitor and control temperature via a Eurotherm detector. Using this setup, we were able to perform annealing experiments under controlled conditions for up to several hours with temperature fluctuations of ± 5°C. Time

taken to heat the sample to the desired temperature was less than 10 s. Annealed samples were quenched by turning off the power to the heating circuit. Even for samples annealed at 1,000°C, quench times were rapid, and samples cooled to below 100°C in about 12 s. All spectra were obtained once annealed samples had cooled down to room temperature. The advantage of this technique is that individually prepared crystals from each of the three batches could be annealed for increasing amounts of time under controlled atmospheres, and spectra obtained after each cycle of heating. By annealing samples under different conditions it is, in theory, possible to mobilize interstitial H, which can be considered as one of the fastest diffusing species in many minerals, as well as slowly annealing out other types of defects, including substitutional and interstitial defects as well as cation and anion vacancies. Therefore, it is possible to determine how H interacts with other types of defect and how annealing affects the overall H affinity of the rutile structure. The further advantage of this technique is that it allows the sample to be studied optically during and after annealing so that any colour changes can also be observed.

Results

Figures 5 and 6 show two representative series of spectra obtained from irradiated and unirradiated rutile after annealing in air. For all samples, annealing experiments were performed from 400 to 1,000°C in 100°C steps. Table 1 gives a summary of the effects of annealing on optical properties and OH absorption bands. Ambient spectra from all samples contained a broad background over the region 4,000–2,500 cm^{-1}. This background is only present in spectra obtained through the heating cell, and disappeared during heating above 100°C for a few seconds. The most likely source of this signal is the heating cell itself, perhaps from trace amounts of water on the surface of the CaF_2 windows. It should also be noted that the spectral resolution is noticeably poorer in spectra obtained through the heating cell compared to spectra shown in Fig. 2, sometimes making it difficult to resolve smaller absorption bands (note that the OH band at 3,375 cm^{-1} is not resolvable in the ambient spectrum in Fig. 6). This is probably due to a combination of several factors including absorption of some of the signal by the components of the heating cell, the slightly smaller sample size used for annealing experiments and the smaller aperture used for obtaining spectra from the annealed samples (constrained by the diameter of the hole in the Pt furnace over which the sample was suspended).

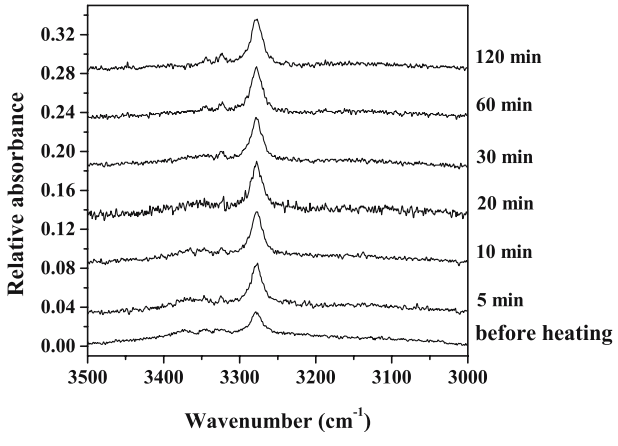

Fig. 5 NIR spectra from an irradiated rutile crystal before heating, and after annealing for increasing amounts of time in air at 500°C (*offset vertically*). A linear background over the region 4,000–2,000 cm^{-1} has been subtracted. Spectra were obtained at 25°C through the heating cell

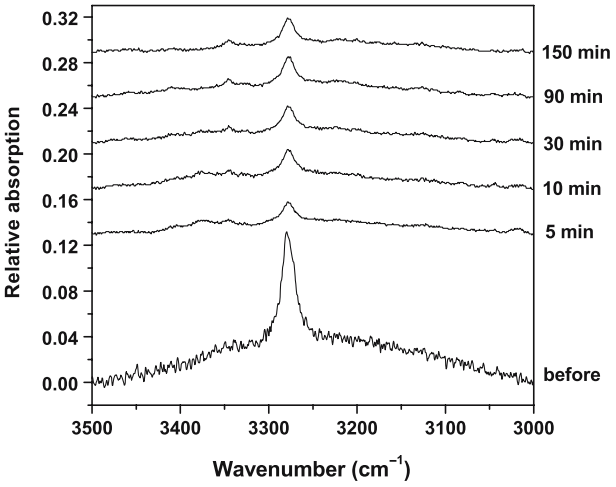

Fig. 6 The IR spectra from a rutile crystal (unirradiated) before heating, and after annealing for increasing amounts of time in air at 500°C (*offset vertically*). A linear background over the region 4,000–2,000 cm^{-1} has been subtracted. Spectra were obtained at 25°C through the heating cell

Discussion

Main OH band at 3,279 cm^{-1}

In all annealing experiments, changes in the intensity of the main OH absorption band at 3,279 cm^{-1} are observed. This band accounts for over 95% of all of the structurally-incorporated H in the rutile samples, and represents the most important H incorporation mechanism in rutile. This band can be assigned to H incorporated close to one of the shared O–O edges, and represents H coupled with reduced Ti on the main octahedral site ($Ti^{/}_{Ti}$) or H not coupled to substitional defects (Bromiley and Hilaret 2005). Changes in the height of the OH band at 3,279 cm^{-1} imply H diffusion into or out of the samples during annealing. Rates of H diffusion are fast, highly temperature dependent, and in a number of experiments can be modeled by simple decay laws. It should be noted that changes in the height of

Table 1 Summary of the effects of annealing rutile samples under oxidizing and reducing conditions at T from 400 to 1,000°C

Sample	Gas	Effects on optical properties	Effect on 3,279 cm^{-1} band	Effect on minor OH bands
Irradiated rutile	Ar–2%H_2	No colour change up to 600°C. Above 700°C samples darken slowly during annealing. Samples opaque after annealing for 5 min at 1,000°C	Rapid H loss even at 500°C. All H lost at 700°C after only 5 min	Not seen
	Air	Samples become lighter during annealing. Rate of colour change is slow, but becomes faster at higher T	Increase in H content to equilibrium value at all T. Rate of H increase is T dependent	OH bands at 3,325 and 3,345 cm^{-1} appear during annealing up to 700°C. At 800°C and above, only band at 3,325 cm^{-1} is seen. Increase in band heights is very slow, and does not reach equilibrium even after 6 h heating at 1,000°C
Unirradiated rutile	Ar–2%H_2	No colour change at 500°C. At 700°C and higher, crystals darken slowly during prolonged annealing	Rapid H loss. At lower T, H content is reduced to an equilibrium value. At 800°C and above, all H is lost. Rate of H lost is T dependent	Band at 3,345 cm^{-1} noted during prolonged annealing at 500 and 600°C, but is barely resolvable. Band at 3,325 cm^{-1} not seen
	Air	Samples become lighter during annealing. Colour change much more rapid at higher T	Rapid H loss, and re-equilibriation at lower value all T	Slow increase in the height of 3,345 cm^{-1} band after prolonged annealing. 3,325 cm^{-1} band only noted after heating at 800°C and above

the minor OH absorption bands at 3,325 and 3,345 cm^{-1} are considerably slower, usually by at least one order of magnitude. This would appear to indicate that these two OH bands represent H coupled to other types of defects, and that by contrast, the 3,279 cm^{-1} band represents uncoupled H. This is supported by the fact that changes in the height of the 3,279 cm^{-1} absorption band occur at all temperatures and are unrelated to colour changes. We have shown above that optical absorption in rutile is due to Ti reduction; that is, to the presence of Ti^{3+} and IVCT. This indicates that changes in the 3,279 cm^{-1} OH band appear to be unrelated to reduction/oxidation of Ti.

H diffusion into irradiated samples annealed in air requires an additional source of H_2O. Possibly, this could be from the air, and may represent dissociation of water at the rutile surface, coupled destruction of an oxygen vacancy and creation of H interstitials:

$$H_2O\,(\text{gas}) + V_O^{\cdot\cdot}\,(\text{rutile}) = O_O\,(\text{rutile}) + 2H_i^{\cdot}\,(\text{rutile}). \quad (1)$$

This implies that H diffusion is coupled with $V_O^{\cdot\cdot}$ diffusion out of the samples/O^{2-} diffusion into the samples, which would be expected under oxidizing annealing conditions. Alternatively, the source of interstitial H could be from H related species already adsorbed on rutile surfaces, such as the (001) surface, which has a high affinity for absorption of H_2O-related species (van der Berg et al. 2003). Before annealing, rutile crystals were prepared by polishing two parallel faces. However, a significant part of the original crystal surface was not polished and could, in theory, retain a small amount of water or hydroxyl during annealing (up to several ppm H_2O by weight), which acts as a source for H diffusion into the samples under the appropriate conditions. Equation (1) could also be used to explain H diffusion following dissociation of water adsorbed on rutile surfaces. A third potential source of hydrogen could be channels in the rutile structure. During irradiation, H contents of reduced rutile decrease markedly. However, this assessment is based on measurements of OH absorption band intensity using infrared spectroscopy. OH groups are IR active because they have a significant dipole moment. It is possible that during irradiation, changes to the electronic structure of reduced rutile favour H incorporation as H_2 contained in the large (up to 3.326 Å across) channels present in the rutile structure. Interchannel H_2 would not be IR active unless the H_2 was in a low-symmetry environment, which distorted the electron shell in such a way that a dipolar momentum was induced. However, H_2 molecules should be detectable using Raman spectroscopy. According to Schmidt et al. (1998), trapped H_2 molecules would have a strong Raman active mode between 4,100 and 4,200 cm^{-1}. This was not detected in Raman spectra obtained from the irradiated rutile samples in this study, although because of the small sample size and relatively poor signal to noise ratio, the existence of a small H_2 Raman band cannot be completely discounted. Channels in the rutile structure consist of adjoining interstitial sites, and run parallel to [001]. Migration of H to rutile channels and then combination to form various H-related species could occur during irradiation. This appears a favourable mechanism for H loss because it does not rely on H diffusion through the bulk of the sample. Mass transport

of H to crystal surfaces by hopping of interstitial H from one oxygen site to the next might be considered unfavourable at the temperatures experienced by samples during irradiation, which were probably below 60°C. Once H-related species were present in rutile channels, transport to crystal surfaces would also be possible. Diffusion of inter-channel species in rutile was noted by Kingsbury et al. (1968), who studied fast Li diffusion via hopping of Li between two distinct sites in rutile channels. A second reason for considering inter-channel H_2 in the irradiated rutile is that it provides a ready, local source for H during annealing in air. H contents of annealed samples increase rapidly, which might be more consistent with a local source of H as opposed to H diffusion from rutile surfaces.

Changes in the intensity of the 3,279 cm^{-1} band are noted in all annealing experiments. This is probably related to the concentration of $V_O^{\cdot\cdot}$ defects. Reduction in the H affinity of irradiated rutile was explained on the basis of an increase in the number of $V_O^{\cdot\cdot}$ resulting in an increase in the amount of O overbonding, charge imbalance and/or direct breaking of OH bonds. Annealing irradiated rutile in air presumably anneals out some of the $V_O^{\cdot\cdot}$ created during irradiation. Conversely, annealing irradiated rutile in Ar–2%H_2 results in the further creation of $V_O^{\cdot\cdot}$, leading to a further decrease in the amount of interstitial H. Alternatively, annealing under reducing conditions could merely provide sufficient energy for re-equilibriation of the H content of rutile samples following intense neutron irradiation. This would imply that H contents of irradiated rutile samples were not equilibrium values, which might be expected due to the low temperatures encountered by the samples during irradiation. It should be noted that annealing experiments clearly demonstrate that broad trends in H affinity are unrelated to colour changes, and therefore, presumably to Ti^{3+}/Ti^{4+} redox reactions. It might also be expected that an increase in the amount of $Ti_i^{\cdot\cdot}$ would also result in a slight decrease in H affinity in rutile. However, any such trends are not seen in annealing experiments, indicating that the concentration of $V_O^{\cdot\cdot}$ has a much greater affect on H affinity in rutile than the presence of interstitial cations.

Minor OH absorption bands

Spectra from some of the annealed samples contain two additional absorption bands at 3,325 and 3,345 cm^{-1}. Changes in intensity of these small bands are difficult to ascertain because they are often difficult to resolve. However, on the basis of the present results several broad trends can be identified. Firstly, the band at 3,375 cm^{-1} is never seen in spectra from annealed samples, even when H contents increase significantly during annealing. This implies that this band is only stable under the conditions of high-pressure synthesis, and may either represent an additional H incorporation mechanism, or coupling of H with some other type of defect only stable at high pressure. In annealed spectra, the only additional OH bands are those at 3,325 and 3,345 cm^{-1}. Changes in the height of these two bands are very slow (about an order of magnitude slower than changes in the height of the main OH band at 3,279 cm^{-1}), suggesting that they can be assigned to H coupled with other types of defect. Furthermore, each of the two bands appear to be due to H associated with different defects, because changes in height of each band are different at different T. It is possible that different temperature behaviour of the two bands could be related to changes in oxidation/reduction of Ti^{3+}/Ti^{4+}, which is also T dependent.

These minor OH bands could also represent H incorporated via different mechanisms. For example, on the basis of first-principles calculations, Koudriachova et al. (2004) suggested H is incorporated in the rutile structure in a channel centre site (i.e. vibration of an O–H bond towards one of the large interstitial sites in the structure). H incorporated via such a mechanism could also form a defect cluster, if, as suggested by Koudriachova et al. (2004), it remained associated with a trivalent cation on the adjacent octahedral site (i.e. $Ti_{Ti}^{/}$). The relative stability of this coupled defect could differ from that of H incorporated via the Swope et al. (1995) model, and might explain some of the differences in the behaviour of the small OH bands in the rutile spectra, as a function of annealing temperature and pressure.

Reduction and oxidation of Ti

Optical absorption in reduced rutile is mainly due to Ti^{3+} Ti^{4+} IVCT, so it is possible to use colour changes as an indicator for Ti redox changes. Annealing experiments on unirradiated and irradiated rutile demonstrate that a specific energy is required to reduce Ti^{4+}. For both sets of samples, annealing in Ar–2%H_2 only results in reduction, and an increase in optical absorption, at T > 700°C. In contrast, annealing in air results in a colour change, and Ti^{3+} oxidation, at all temperatures. Changes in the height of the 3,279 cm^{-1} OH band relate to H affinity of rutile under different conditions. These changes are unrelated to Ti redox reactions, and are presumably governed by the concentration of $V_O^{\cdot\cdot}$ defects. If true, this has implications for the relative stabilities and diffusivities of Ti^{3+} and $V_O^{\cdot\cdot}$ defects. Firstly, under reducing conditions, the energy required to create $V_O^{\cdot\cdot}$ is lower than that required to further reduce rutile. This is consistent with calculated energies of different point defects and defect clusters in TiO_2 (Catlow et al. 1982). Secondly, under oxidizing conditions, fast rates of H diffusion suggest rates of $V_O^{\cdot\cdot}$ diffusion are much faster than rates of Ti^{3+} defect diffusion. This is consistent with experimental studies of O diffusion in rutile, which show that oxygen diffusion coupled with diffusion of oxygen vacancies is significantly faster, and has a significantly lower activation energy, than diffusion coupled with interstitials (Moore et al. 1998).

In several annealing experiments, the 3,345 cm^{-1} band appears in NIR spectra after prolonged annealing

when Ti^{3+} defects are stable. This suggests that the 3,345 cm^{-1} band is due to H coupled with Ti^{3+}, most likely on the octahedral site, giving rise to the defect cluster Ti'_{Ti}–$H^{\cdot}_{i}$. Growth of the OH band at 3,345 cm^{-1} would signify coupling of two different defects that become mobilized at elevated T. During annealing, H will be a highly mobile species. Additionally, mobility of Ti^{3+} defects at elevated temperature was demonstrated by Henderson (1999), who used isotope doped rutile samples to demonstrate that bulk diffusion of Ti^{3+} to the rutile surface was activated above 430°C (in air). To test this assignment, we performed an additional annealing experiment in Ar–2%H_2 at 500°C using unirradiated rutile. During prolonged annealing, a slow increase in the peak height of the 3,345 cm^{-1} absorption band occurred, as would be expected due to coupling of mobile $H^{\cdot}_{i}$ with Ti'_{Ti} defects, even though the overall H content of the sample decreased. The gas supply was then turned off, and we continued annealing the sample in the air. This led to a reduction in the height of the 3,345 cm^{-1} band, despite the fact that the overall H content of the sample then increased. This change was also accompanied by a reduction in optical absorption of the sample, implying Ti^{3+} oxidation. These observations are consistent with assignment of the 3,345 cm^{-1} OH band to coupled Ti'_{Ti}–$H^{\cdot}_{i}$ defects.

Correlation between changes in optical absorption and the height of the 3,345 cm^{-1} band during some annealing experiments would imply that the energy required to oxidize isolated Ti^{3+} is the same as that required to oxidize Ti^{3+} coupled to interstitial H. However, during annealing of unirradiated rutile in air, the 3,345 cm^{-1} band persists above the temperature required for Ti^{3+} oxidation, implying that under these conditions, coupled Ti'_{Ti}–$H^{\cdot}_{i}$ defects are more stable than isolated $Ti^{\cdot\cdot\cdot\cdot}_{i}$. In fact, we observed that in a number of instances, the relative stabilities of certain defects were different in oxidized and reduced rutile. Similar observations have been made in previous studies. Aono and Hasiguti (1993) used EPR spectroscopy to study different types of defect formed in strongly reduced rutile, and concluded that Ti interstitials often form coupled pairs. Furthermore, they found evidence for large-scale ordering of Ti interstitials in cooperation with oxygen vacancies to form {121} planar defects. On the basis of electron absorbance spectroscopy, Lu et al. (2001) suggested that reduced rutile contained the defect centre Ti'_{Ti}–$V^{\cdot\cdot}_{O}$ (i.e. reduced Ti on the main octahedral site coupled to an oxygen vacancy on one of the neighbouring O sites). A number of recent studies have also found evidence for ordering of Ti^{3+} defects, resulting in the formation of crystallographic shear planes (see Diebold 2003 for a general review). Clustering of defects in rutile under different conditions is, therefore, expected, and is likely to be strongly dependent on defect concentration. This will lead to added difficulties in interpreting relative stabilities of different defects in reduced, irradiated and annealed rutile samples.

Effects of pressure on H solubility

Annealing experiments performed on unirradiated rutile also demonstrate rapid re-equilibriation of H contents, consistent with H diffusion. However, during annealing under both oxidizing and reducing conditions, there is a decrease in the amount of interstitial H incorporated. This result can only be interpreted in terms of the effect of pressure on hydrogen solubility. Presumably, H solubility in rutile is markedly lower at ambient pressure than at 1.5 GPa, and the effect of annealing samples is to re-equilibriate H contents at much lower values. Bromiley et al. (2004a) demonstrated that H solubility in Fe_2O_3-doped rutile is also strongly pressure dependent, and increases significantly from 0.5 to 2.0 GPa. They also noted that trends in H solubility in rutile were not related to trends in Fe_2O_3 solubility, even though the main charge-balancing mechanism for H incorporation was substitution for Fe^{3+} for Ti^{4+}. This suggests that changes in H affinity in rutile are not necessarily related to the concentration of Ti^{3+} defects, even though reduction of Ti^{4+} must provide the dominant mechanism for charge-balancing H incorporation. This is consistent with the results of annealing experiments, which show that the concentration of $V^{\cdot\cdot}_{O}$ has a much greater influence of H affinity.

Summary

The effects of neutron irradiation and post-irradiation annealing of reduced rutile demonstrate that:

1. Optical absorption is mainly due to Ti^{3+} Ti^{4+} IVCT, with electron sharing between Ti on adjacent octahedral and interstitial sites, presumably also coupled with absorption due to Ti^{3+} crystal field transitions.
2. The main effect of neutron irradiation is production of oxygen vacancies, which results in a marked reduction in H affinity in rutile and reduction in the intensity of optical absorption.
3. Most H in rutile gives rise to an IR active OH-stretching band at 3,279 cm^{-1}, presumably due to H incorporated close to the shared O–O edge. Annealing experiments suggest that this band is due to interstitial H not coupled to other defects (such as reduced Ti on adjacent octahedral sites). Rates of H diffusion are fast, and may be coupled to fast diffusion of $V^{\cdot\cdot}_{O}$.
4. A number of additional, minor OH bands are noted in rutile spectra. A band at 3,345 cm^{-1} could be due to H coupled with Ti^{3+} on adjacent octahedral sites [$H^{\cdot}_{i}$–Ti'_{Ti}]. Other bands could be due to H incorporated on other sites, for example, OH vibration towards the large interchannel sites in rutile, also presumably coupled with other substitutional defects.
5. H affinity in rutile decreases with increasing concentration of $V^{\cdot\cdot}_{O}$, but increases with increasing P.

Annealing experiments demonstrate the relative stability of different defects in reduced rutile. However, it is not possible to quantify the stability of different defects based on high T behaviour. In fact, differences are noted in the relative stability of different defects between oxidized and reduced rutile samples. This is most likely due to ordering of defects in rutile, as has been noted in a number of other studies.

Acknowledgements This work was funded by the Bayersiches Geoinstitut visiting scientists program (to GDB) and by Alexander von Humboldt foundation (to AAS). The authors thank Dr. N. N. Dogadkin (Vernadsky Institute of Geochemistry) for performing neutron irradiation experiments. Hans Keppler is thanked for useful comments regarding H_2 measurements. Comments by two anonymous reviewers greatly improved the quality of this paper.

References

Aono M, Hasiguti R (1993) Interaction and ordering of lattice defects in oxygen-deficient rutile TiO_{2-x}. Phys Rev B 48(17):12406–12414

van der Berg A, Gora L, Jansen J, Maschmeyer T (2003) Improvement of zeolite NaA nucleation sites on (001) rutile by means of UV radiation. Microporous Mesoporous Materials 66:303–309

Bromiley GD, Keppler H (2004) An experimental investigation of hydroxyl solubility in jadeite and Na-rich pyroxenes. Contrib Mineral Petrol 147:189–200

Bromiley GD, Hilaret N (2005) An investigation of hydrogen and minor element incorporation in synthetic rutile. Mineral Mag 69(3):345–358

Bromiley GD, Hilaret N, McCammon C (2004a) Solubility of hydrogen and ferric iron in rutile and TiO_2 (II): Implications for phase assemblages during ultrahigh-pressure metamorphism and for the stability of silica polymorphs in the lower mantle. Geophys Res Lett 31:L04610

Bromiley GD, Keppler H, McCammon C, Bromiley F, Jacobsen S (2004b) Hydrogen solubility and speciation in natural, gem-quality chromian diopside. Am Mineral 89:941–949

Buck EC (1995) The effects of electron irradiation of rutile. Rad Effects Defects Solids 133(2):141–152

Catlow C, James R, Mackrodt W, Stewart R (1982) Defect energies in α-Al_2O_3 and rutile TiO_2. Phys Rev B 25(2):1006–1026

Diebold U (2003) The surface science of titanium dioxide. Surf Sci Rep 48(4–5):53–229

Gonzalez R, Chen Y (2002) Transport of hydrogenic species in crystalline oxides: radiation and electric-field-enhanced diffusion. J Phys Condensed Matter 14(45):R1143–R1173

Hammer V, Beran A (1991) Variations in the OH concentrations of rutile from different geological environments. Mineral Petrol 45:1–9

Henderson M (1999) A surface perspective on self-diffusion in rutile TiO_2. Surf Sci 419:174–187

Kappers LO (1978) Point defects in particle-irradiated single crystals of tetragonal GeO_2. Phys Rev B 17:4199–4206

Katayama I, Hirose K, Yurimoto H, Nakashima S (2003) Water solubility in majoritic garnet in subducting oceanic crust. Geophys Res Lett 30(22):2155

Khomenko V, Langer K, Rager H, Fett A (1998) Electronic absorption by Ti^{3+} ions and electronic delocalization in synthetic blue rutile. Phys Chem Mineral 25:338–346

Kingsbury PW, Ohlsen W, Johnson OW (1968) Defects in rutile III. Diffusion of interstitial ions. Phy Rev B 175:1099–1101

Kohn S, Brooker R, Frost D, Slesinger A, Wood B (2002) Ordering of hydroxyl defects in hydrous wadsleyite (beta-Mg_2SiO_4). Am Mineral 87(2–3):293–301

Koudriachova M, de Leeuw S, Harrison N (2004) First-principles study of H intercalation in rutile TiO_2. Phys Rev B 70:165421

Kröger FA, Vink HJ (1956) Relations between the concentrations of imperfections in crystalline solids. In: Seitz F, Turnball D (eds) Solid state physics: advances and applications, vol 3. Academic, New York, pp 307–435

Lager G, von Dreele R (1996) Neutron powder diffraction study of hydrogarnet to 9.0 GPa. Am Mineral 81(9–10):1097–1104

Lehman C (1977) Interaction of radiation with solids and elementary defect production. In: Defects in crystalline solids, vol 10. North Holland Publishing Company, Amsterdam, 341 pp

Lu T-C, Wu S-Y, Lin L-B, Zheng W-C (2001) Defects in the reduced rutile single crystal. Physica B 304:147–151

Lu T-C, Lin L-B, Wu S-Y, Chen J, Zhang Y-Y (2002a) Influence of neutron irradiation and its post-annealing on optical absorption of rutile. Nucl Instrum Methods Phys Res B 191:236–240

Lu T-C, Lin L-B, Wu S-Y, Xu X-C, Cheng G (2002b) Influence of proton implantation on optical absorption of rutile. Surf Coatings Technol 158–159:431–435

Moore D, Cherniak D, Watson E (1998) Oxygen diffusion in rutile from 750 to 1,000°C and 0.1 to 1,000 MPa. Am Mineral 83:700–711

Schmidt BC, Holtz FM, Bény J-M (1998) Incorporation of H_2 in vitreous silica, qualitative and quantitative determination from Raman and infrared spectroscopy. J Non-Crystalline Solids 240:91–103

Swope R, Smyth J, Larson A (1995) H in rutile compounds: I. Single-crystal neutron and X-ray diffraction study of H in rutile. Am Mineral 80:448–453

Thomas BS, Marks NA, Corrales LR, Devanathan R (2005) Threshold displacement energies in rutile TiO_2: a molecular dynamics simulation study. Nucl Instrum Methods Phys Res B 239(3):191–201

Traylor J, Smith H, Nicklow R, Wilkinson M (1971) Lattice dynamics of rutile. Phys Rev B 3(10):3457–3472

Zapunnyy S, Sobolev A, Bogdanov A, Slutsky A, Dmitriev L, Kunin L (1989) An apparatus for high-temperature optical research with controlled oxygen fugacity. Geochim Int 26(2):120–128